arXiv:1405.1198v1 [physics.optics] 6 May 2014

Giant dielectric anisotropy via homogenization

Tom G. Mackay*

School of Mathematics and Maxwell Institute for Mathematical Sciences

University of Edinburgh, Edinburgh EH9 3JZ, UK

and

NanoMM — Nanoengineered Metamaterials Group

Department of Engineering Science and Mechanics

Pennsylvania State University, University Park, PA 16802–6812, USA

Abstract

A random mixture of two isotropic dielectric materials, one composed of oriented spheroidal particles of relative permittivity ϵ_a and the other composed of oriented spheroidal particles of relative permittivity ϵ_b, was considered in the long wavelength regime. The permittivity dyadic of the resulting homogenized composite material (HCM) was estimated using the Bruggeman homogenization formalism. The HCM was an orthorhombic biaxial material if the symmetry axes of the two populations of spheroids were mutually perpendicular and a uniaxial material if these two axes were mutually aligned. The degree of anisotropy of the HCM, as gauged by the ratio of the eigenvalues of the HCM's permittivity dyadic, increased as the shape of the constituent particles became more eccentric. The greatest degrees of HCM anisotropy were achieved for the limiting cases wherein the constituent particles were shaped as needles or discs. In these instances explicit formulas for the HCM anisotropy were derived from the dyadic Bruggeman equation. Using these formulas it was found that the degrees of HCM anisotropy are proportional to $\sqrt{\epsilon_b}$ or ϵ_b, at fixed values of volume fraction and ϵ_a, for $\epsilon_b > \epsilon_a$. Thus, in principle, there is no limit to degree of anisotropy that may be attained via homogenization. In practice, the degree of anisotropy would be limited by the available value of ϵ_b (and/or ϵ_a).

Keywords: Bruggeman homogenization formalism; needle–shaped particles; disc–shaped particles; giant anisotropy

*E–mail: T.Mackay@ed.ac.uk

1 Introduction

While nature provides us with a great many anisotropic materials [1, 2], there are occasions when a material with a specific degree of anisotropy may be required but none is readily available. On such occasions we may turn to engineered composite materials. Rather exotic dielectric anisotropies have been central to recent developments involving nanostructured composite materials which support electromagnetic phenomenons such as negative refraction [3], optical cloaking [4], null reflection [5], and omnidirectional radiation [6], for examples. Most significantly, the incorporation of dielectric anisotropy can enable non–magnetic composite materials to support negative refraction [7, 8]. Another notable area where dielectric anisotropy plays a key role is in the development of material analogues for the electromagnetic properties of certain curved spacetime scenarios, such as rotating black holes [9, 10], Schwarzschild-(anti-)de Sitter spacetime [11], and cosmic spinning strings [12], as well as material analogues of quantum electrodynamic vacuum [13]. In particular, high degrees of dielectric anisotropy are needed to represent regions of large spacetime curvature, close to singularities or event horizons, for examples.

Biaxial or uniaxial anisotropy can be attained by homogenizing composite materials which are composed of oriented constituent particles characterized by certain symmetries, such as cylindrical [8] or ellipsoidal [14] symmetry. In the following, we investigate a means of achieving very high degrees of dielectric anisotropy, in a controllable manner, through the homogenization of remarkably simple component materials, namely isotropic dielectric materials composed of spheroidal particles. The approach taken is based on the well–established Bruggeman homogenization formalism [15, 16].

A note concerning notation: In the following, 3–vectors are single underlined while 3×3 dyadics are double underlined. Unit vectors are signified by the $\hat{}$ symbol. Thus, unit vectors aligned with the coordinate axes are written as $\underline{\hat{x}}$, $\underline{\hat{y}}$ and $\underline{\hat{z}}$. The identity and null 3×3 dyadics are denoted by $\underline{\underline{I}}$ and $\underline{\underline{0}}$, respectively.

2 Homogenization preliminaries

2.1 Component materials

Let us study the homogenization of two isotropic dielectric component materials, namely material a which is characterized by the relative permittivity ϵ_a and material b which is characterized by the relative permittivity ϵ_b. It assumed that the component materials are lossless and that $\epsilon_{a,b} > 0$.[1] Both component materials are particulate in nature; their constituent particles are taken to be spheroidal in shape (and limiting cases of

[1] Homogenization formalisms can yield results which are not physically plausible in the $\epsilon_a \epsilon_b < 0$ regime [17, 18].

these spheroidal shapes are also considered). The component materials are randomly mixed together to form a composite material, with component material a having the volume fraction f_a and material b the volume fraction $f_b = 1 - f_a$. In the composite material, all material a spheroidal particles are assumed to have the same shape and orientation, and likewise all material b spheroidal particles are assumed to have the same shape and orientation. The surface of each constituent spheroidal particle of type a or type b, relative to its centroid, is traced out by the vector

$$\underline{r}_s(\theta,\phi) = \eta\, \underline{\underline{U}}_\ell \bullet \underline{\hat{r}}(\theta,\phi), \qquad (\ell = a, b)\,. \tag{1}$$

Here $\underline{\hat{r}}$ is the radial unit vector with its origin coinciding with the spheroid's centroid; it is specified in terms of the spherical polar coordinates θ and ϕ. The dyadic

$$\underline{\underline{U}}_\ell = \frac{1}{\sqrt{\gamma_\ell}}\left(\underline{\underline{I}} - \underline{\hat{c}}_\ell\,\underline{\hat{c}}_\ell\right) + \gamma_\ell\,\underline{\hat{c}}_\ell\,\underline{\hat{c}}_\ell\,, \qquad (\ell = a, b)\,, \tag{2}$$

characterizes the spheroidal shape and orientation; herein the unit vector $\underline{\hat{c}}_\ell$ is aligned with the spheroid's axis of rotational symmetry. The eccentricity of the spheroid is captured by the positive-valued parameter γ_ℓ; for the degenerate case $\gamma_\ell = 1$ the spheroid takes the form of a sphere. The linear dimensions of the spheroid are fixed by the positive–valued size parameter η.

In the following sections two cases are investigated: (i) the case where the component material a spheroids are aligned perpendicularly to the component material b spheroids (i.e., $\underline{\hat{c}}_a \bullet \underline{\hat{c}}_b = 0$); and (ii) the case where the component material a spheroids and the component material b spheroids have the same alignment (i.e., $\underline{\hat{c}}_a \bullet \underline{\hat{c}}_b = 1$). To be specific, let us choose $\underline{\hat{c}}_a = \underline{\hat{z}}$ and $\underline{\hat{c}}_b = \underline{\hat{y}}$ for case (i), and $\underline{\hat{c}}_a = \underline{\hat{c}}_b = \underline{\hat{z}}$ for case (ii). For simplicity, the eccentricity of the component material a spheroids is taken to be the same as that for the component material b spheroids; accordingly, we introduce the eccentricity parameter $\gamma \equiv \gamma_a = \gamma_b$. Schematic representations of these cases (i) and (ii) are provided in Fig. 1.

2.2 Homogenized composite material

The composite material described in §2.1 may be regarded as being effectively homogeneous provided that the constituent spheroidal particles are much smaller than the wavelength(s) under consideration. Unlike the component materials, the corresponding homogenized composite material (HCM) is an anisotropic dielectric material [19]. The anisotropic nature of the HCM stems from the geometry of its oriented spheroidal constituent particles. For both cases (i) and (ii), the relative permittivity dyadic of the HCM may be represented by the general form

$$\underline{\underline{\epsilon}}_{HCM} = \epsilon_x\,\underline{\hat{x}}\,\underline{\hat{x}} + \epsilon_y\,\underline{\hat{y}}\,\underline{\hat{y}} + \epsilon_z\,\underline{\hat{z}}\,\underline{\hat{z}}\,. \tag{3}$$

For case (i) there are three distinct relative permittivity parameters, namely ϵ_x, ϵ_y and ϵ_z, and the corresponding HCM is an orthorhombic biaxial material. For case (ii) there are only two distinct relative

permittivity parameters, namely ϵ_x and ϵ_z, since here $\epsilon_x = \epsilon_y$; and the corresponding HCM is a uniaxial dielectric material.

The relative permittivity dyadic of the HCM may be estimated by means of the widely–used Bruggeman homogenization formalism [15, 16]. This process involves extracting $\underline{\underline{\epsilon}}_{HCM}$ from the dyadic Bruggeman equation [19]

$$f_a \, \underline{\underline{\alpha}}_a + f_b \, \underline{\underline{\alpha}}_b = \underline{\underline{0}}, \tag{4}$$

which is expressed in terms of the polarizability density dyadics

$$\underline{\underline{\alpha}}_\ell = \left(\epsilon_\ell \underline{\underline{I}} - \underline{\underline{\epsilon}}_{HCM} \right) \cdot \left[\underline{\underline{I}} + \underline{\underline{D}}_\ell \cdot \left(\epsilon_\ell \underline{\underline{I}} - \underline{\underline{\epsilon}}_{HCM} \right) \right]^{-1}, \qquad (\ell = a, b). \tag{5}$$

The depolarization dyadics $\underline{\underline{D}}_\ell$ herein are given by the double integrals [20, 21]

$$\underline{\underline{D}}_\ell = \frac{1}{4\pi} \int_\phi^{2\pi} d\phi \int_\theta^{\pi} d\theta \, \sin\theta \, \frac{\left(\underline{\underline{U}}_\ell^{-1} \cdot \hat{\underline{r}} \right) \left(\underline{\underline{U}}_\ell^{-1} \cdot \hat{\underline{r}} \right)}{\left(\underline{\underline{U}}_\ell^{-1} \cdot \hat{\underline{r}} \right) \cdot \underline{\underline{\epsilon}}_{HCM} \cdot \left(\underline{\underline{U}}_\ell^{-1} \cdot \hat{\underline{r}} \right)}, \qquad (\ell = a, b) \, . \tag{6}$$

The components of $\underline{\underline{D}}_\ell$ may be expressed in terms of incomplete elliptic functions when the HCM is an orthorhombic biaxial material (i.e., case (i)) [22], and in terms of inverse hyperbolic and trigonometric functions when the HCM is a uniaxial material (i.e., case (ii)) [20]; further details are provided in the Appendix.

Due to the nonlinearity of the dyadic Bruggeman equation (4), numerical techniques are usually needed to deliver $\underline{\underline{\epsilon}}_{HCM}$ when the HCM is an anisotropic (or bianisotropic) material [23]. However, as presented in §4, for certain limiting cases explicit solutions can be derived.

3 Spheroidal constituent particles

By means of some representative numerical examples, let us explore the anisotropy that may be induced through homogenizing the assembly of oriented spheroidal particles described in §2.1. We focus on the quantities ϵ_x/ϵ_y, ϵ_y/ϵ_z and ϵ_x/ϵ_z which provide measures of the degrees of anisotropy exhibited by the HCM.

Suppose that $\epsilon_a = 1.5$ and $\epsilon_b = 12$. For case (i), wherein $\hat{\underline{c}}_a = \hat{\underline{z}}$ and $\hat{\underline{c}}_b = \hat{\underline{y}}$, the quantities ϵ_x/ϵ_y, ϵ_y/ϵ_z and ϵ_x/ϵ_z are plotted versus the eccentricity parameter $\gamma \in (0.1, 6)$ in Fig. 2. Here the volume fraction $f_a = 0.7$ (green, dashed curves), 0.4 (red, solid curves) and 0.1 (blue, broken dashed curves). The magnitudes of ϵ_x/ϵ_y, ϵ_y/ϵ_z and ϵ_x/ϵ_z diverge from unity as γ diverges from unity. While the HCM is clearly biaxial, for $f_a = 0.1$ the quantity ϵ_x/ϵ_y is approximately equal to one at all values of γ considered; this indicates that when the concentration of component material a is very small, the electromagnetic properties of the HCM

are very much dominated by component material b and accordingly the HCM is nearly uniaxial. At $\gamma = 1$, we have $\epsilon_x = \epsilon_y = \epsilon_z$ and the HCM is isotropic.

We repeat the calculations of Fig. 2 for case (ii), wherein $\underline{\hat{c}}_a = \underline{\hat{c}}_b = \underline{\hat{z}}$. The anisotropy parameter ϵ_y/ϵ_z ($\equiv \epsilon_x/\epsilon_z$) is plotted versus γ in Fig. 3. The trends in Fig. 3 are similar to those in Fig. 2, but for Fig. 3 the maximum values of ϵ_y/ϵ_z are larger than the maximum values of ϵ_x/ϵ_y, ϵ_y/ϵ_z and ϵ_x/ϵ_z for Fig. 2; and likewise the minimum values of ϵ_y/ϵ_z are smaller than the minimum values of ϵ_x/ϵ_y, ϵ_y/ϵ_z and ϵ_x/ϵ_z for Fig. 2. Thus, we deduce that greater degrees of anisotropy can be achieved when the alignments of the two types of constituent spheroids are the same as compared to the corresponding scenario when the alignments of the two types of constituent spheroids are mutually perpendicular.

For both cases (i) and (ii), the HCM becomes more anisotropic as the constituent particles become more eccentric in shape. However, it would appear from Figs. 2 and 3 that there are limits upon the degrees of anisotropy that can be achieved through varying the eccentricity parameter γ and that these limits depend upon the volume fractions of the component materials. We pursue this matter in §4.

4 Limits to anisotropy

What is the greatest degree of anisotropy than can be achieved by homogenizing an assembly of oriented spheroidal particles? In order to address this question, the limits $\gamma \to \infty$ and $\gamma \to 0$ are considered in the following §4.1 and §4.2, respectively. The depolarization dyadics degenerate to simple forms in these limits, as has been demonstrated in earlier works by a direct analysis of Eqs. (6) [24] or by considering the corresponding eigenfunction expansion cast in cylindrical coordinates [25]. These simplified forms for the depolarization dyadics render the dyadic Bruggeman equation (4) amenable to analysis.

4.1 Needle–shaped constituent particles

In the limit $\gamma \to \infty$ the constituent particles may be regarded as needle–shaped. For case (i) wherein $\underline{\hat{c}}_a = \underline{\hat{z}}$ and $\underline{\hat{c}}_b = \underline{\hat{y}}$, the depolarization dyadics (6) reduce to [24]

$$\left.\begin{aligned} \underline{\underline{D}}_a &= \frac{1}{\epsilon_x - \epsilon_y}\left[\left(1 - \sqrt{\frac{\epsilon_y}{\epsilon_x}}\right)\underline{\hat{x}}\,\underline{\hat{x}} + \left(\sqrt{\frac{\epsilon_x}{\epsilon_y}} - 1\right)\underline{\hat{y}}\,\underline{\hat{y}}\right] \\ \underline{\underline{D}}_b &= \frac{1}{\epsilon_z - \epsilon_x}\left[\left(\sqrt{\frac{\epsilon_z}{\epsilon_x}} - 1\right)\underline{\hat{x}}\,\underline{\hat{x}} + \left(1 - \sqrt{\frac{\epsilon_x}{\epsilon_z}}\right)\underline{\hat{z}}\,\underline{\hat{z}}\right] \end{aligned}\right\}. \tag{7}$$

We investigate numerically the corresponding estimates provided by the Bruggeman homogenization formalism. As for Figs. 2 and 3, let us fix $\epsilon_a = 1.5$. The quantities ϵ_x/ϵ_y, ϵ_y/ϵ_z and ϵ_x/ϵ_z are plotted versus the

relative permittivity $\epsilon_b \in (0.01, 200)$ in Fig. 4. As previously, the volume fraction $f_a = 0.7$ (green, dashed curves), 0.4 (red, solid curves) and 0.1 (blue, broken dashed curves). The magnitudes of ϵ_x/ϵ_y, ϵ_y/ϵ_z and ϵ_x/ϵ_z diverge from unity as ϵ_b diverges from 1.5 (the value of ϵ_a). In the limit $\epsilon_b \to 1.5$ the HCM becomes an isotropic dielectric material, regardless of the volume fraction. For the range of ϵ_b and f_a values considered in Fig. 4, the magnitudes of ϵ_x/ϵ_y, ϵ_y/ϵ_z and ϵ_x/ϵ_z lie within the interval $(0.15, 4.4)$.

Turning to case (ii) wherein $\underline{\hat{c}}_a = \underline{\hat{c}}_b = \underline{\hat{z}}$, the depolarization dyadics (6) reduce to

$$\underline{\underline{D}}_\ell = \frac{1}{2\epsilon_x}\left(\underline{\hat{x}}\,\underline{\hat{x}} + \underline{\hat{y}}\,\underline{\hat{y}}\right), \qquad (\ell = a, b). \tag{8}$$

These particularly simple forms for $\underline{\underline{D}}_{a,b}$ allow an explicit solution to be extracted from the dyadic Bruggeman equation (4). Thus, we find

$$\left.\begin{array}{l} \epsilon_x = \epsilon_y = \dfrac{(f_b - f_a)(\epsilon_b - \epsilon_a) + \sqrt{\left[(f_b - f_a)(\epsilon_b - \epsilon_a)\right]^2 + 4\epsilon_a\epsilon_b}}{2} \\ \\ \epsilon_z = f_a\epsilon_a + f_b\epsilon_b \end{array}\right\}. \tag{9}$$

Let us illustrate the anisotropic nature of the HCM by repeating the calculations of Fig. 4 but with $\underline{\hat{c}}_a = \underline{\hat{c}}_b = \underline{\hat{z}}$. The corresponding plots for the quantity ϵ_y/ϵ_z are presented in Fig. 5. We see that the magnitude of ϵ_y/ϵ_z decreases steadily from unity as ϵ_b diverges from 1.5 (the value of ϵ_a). Thus, the HCM becomes increasingly anisotropic as ϵ_b deviates from ϵ_a. For the range of ϵ_b and f_a values considered in Fig. 5, the magnitude of ϵ_y/ϵ_z lies within the interval $(0.05, 1)$.

Further insight into this matter may be gained by considering the expressions for ϵ_y and ϵ_z given in Eqs. (9). Combining these expressions for the instance $f_a = f_b = 0.5$, we find

$$\frac{\epsilon_z}{\epsilon_y} = \frac{1}{2}\left(\sqrt{\frac{\epsilon_a}{\epsilon_b}} + \sqrt{\frac{\epsilon_b}{\epsilon_a}}\right) \to \infty \quad \text{as} \quad \epsilon_b \to \left\{\begin{array}{l} 0 \\ \infty \end{array}\right. \qquad \text{for fixed } \epsilon_a. \tag{10}$$

That is, the degree of anisotropy, as gauged by ϵ_z/ϵ_y, can increase without limit as ϵ_b increasingly deviates from ϵ_a, and the degree of anisotropy is proportional to $\sqrt{\epsilon_b}$ for $\epsilon_b > \epsilon_a$ and proportional to $1/\sqrt{\epsilon_b}$ for $\epsilon_b < \epsilon_a$.

4.2 Disc–shaped constituent particles

In the limit $\gamma \to 0$ the constituent particles may be regarded as disc–shaped. The corresponding depolarization dyadics (6), for case (i) wherein $\underline{\hat{c}}_a = \underline{\hat{z}}$ and $\underline{\hat{c}}_b = \underline{\hat{y}}$, reduce to [24]

$$\left.\begin{array}{l} \underline{\underline{D}}_a = \dfrac{1}{\epsilon_z}\underline{\hat{z}}\,\underline{\hat{z}} \\ \\ \underline{\underline{D}}_b = \dfrac{1}{\epsilon_y}\underline{\hat{y}}\,\underline{\hat{y}} \end{array}\right\}. \tag{11}$$

For these simple depolarization dyadic forms, the following explicit solution can be extracted from the dyadic Bruggeman equation (4):

$$\left.\begin{aligned} \epsilon_x &= f_a\epsilon_a + f_b\epsilon_b \\ \epsilon_y &= \frac{(f_b - f_a)\,\epsilon_b + \sqrt{(f_b - f_a)^2\,\epsilon_b^2 + 4f_a f_b \epsilon_a \epsilon_b}}{2f_b} \\ \epsilon_z &= \frac{(f_b - f_a)\,\epsilon_a + \sqrt{(f_b - f_a)^2\,\epsilon_a^2 + 4f_a f_b \epsilon_a \epsilon_b}}{2f_a} \end{aligned}\right\}. \tag{12}$$

Let us illustrate this solution numerically. As for Figs. 2–5, we set $\epsilon_a = 1.5$. The quantities ϵ_x/ϵ_y, ϵ_y/ϵ_z and ϵ_x/ϵ_z are plotted versus the relative permittivity $\epsilon_b \in (0.01, 200)$ in Fig. 6. As previously, the volume fraction $f_a = 0.7$ (green, dashed curves), 0.4 (red, solid curves) and 0.1 (blue, broken dashed curves). The general trends are similar to those exhibited in Figs. 4 for needle–shaped particles; that is, the magnitudes of ϵ_x/ϵ_y, ϵ_y/ϵ_z and ϵ_x/ϵ_z diverge from unity as ϵ_b diverges from 1.5 (the value of ϵ_a), regardless of the volume fraction, with the HCM becoming an isotropic dielectric material in the limit $\epsilon_b \to 1.5$. For the range of ϵ_b and f_a values considered in Fig. 6, the magnitudes of ϵ_x/ϵ_y, ϵ_y/ϵ_z and ϵ_x/ϵ_z lie within the interval $(0.2, 4.4)$.

We can better appreciate the anisotropic nature of the HCM here by considering the expressions for ϵ_x, ϵ_y and ϵ_z given in Eqs. (12) for the instance $f_a = f_b = 0.5$. We find that

$$\frac{\epsilon_x}{\epsilon_y} = \frac{\epsilon_x}{\epsilon_z} = \frac{1}{2}\left(\sqrt{\frac{\epsilon_a}{\epsilon_b}} + \sqrt{\frac{\epsilon_b}{\epsilon_a}}\right) \to \infty \quad \text{as} \quad \epsilon_b \to \left\{ \begin{array}{l} 0 \\ \infty \end{array} \right. \qquad \text{for fixed } \epsilon_a, \tag{13}$$

and $(\epsilon_y/\epsilon_z) = 1$. That is, the degree of anisotropy, as gauged by ϵ_x/ϵ_y and ϵ_x/ϵ_z, can increase without limit as ϵ_b increasingly deviates from ϵ_a, and the degree of anisotropy is proportional to $\sqrt{\epsilon_b}$ for $\epsilon_b > \epsilon_a$ and proportional to $1/\sqrt{\epsilon_b}$ for $\epsilon_b < \epsilon_a$.

Lastly we turn to case (ii) wherein $\underline{\hat{c}}_a = \underline{\hat{c}}_b = \underline{\hat{z}}$. The depolarization dyadics (6) simplify to [24]

$$\underline{\underline{D}}_\ell = \frac{1}{\epsilon_z}\,\underline{\hat{z}}\,\underline{\hat{z}}, \qquad (\ell = a, b)\,, \tag{14}$$

and the corresponding solution to the dyadic Bruggeman equation (4)

$$\left.\begin{aligned} \epsilon_x &= \epsilon_y = f_a\epsilon_a + f_b\epsilon_b \\ \epsilon_z &= \frac{\epsilon_a\epsilon_b}{f_b\epsilon_a + f_a\epsilon_b} \end{aligned}\right\} \tag{15}$$

emerges. We repeat the calculations of Fig. 6 but with $\underline{\hat{c}}_a = \underline{\hat{c}}_b = \underline{\hat{z}}$. The corresponding plots of ϵ_y/ϵ_z versus ϵ_b are presented in Fig. 7. As in Fig. 6, the magnitudes ϵ_y/ϵ_z in Fig. 7 deviate from unity as ϵ_b deviates from 1.5 (the value of ϵ_a), but the rates of growth of the ϵ_y/ϵ_z curves in Fig. 7 are greater that those for the corresponding curves in Fig. 6. For the range of ϵ_b and f_a values considered in Fig. 7, the magnitudes of ϵ_y/ϵ_z lie within the interval $(1, 37)$.

As previously, let us consider the expressions for ϵ_y and ϵ_z given in Eqs. (15) for the instance $f_a = f_b = 0.5$. We find that

$$\frac{\epsilon_y}{\epsilon_z} = \frac{1}{4}\frac{\left(\epsilon_a + \epsilon_b\right)^2}{\epsilon_a \epsilon_b} \to \infty \quad \text{as} \quad \epsilon_b \to \begin{cases} 0 \\ \infty \end{cases} \quad \text{for fixed } \epsilon_a. \tag{16}$$

That is, the degree of anisotropy, as gauged by ϵ_y/ϵ_z, can increase without limit as ϵ_b increasingly deviates from ϵ_a, and the degree of anisotropy is proportional to ϵ_b for $\epsilon_b > \epsilon_a$ and proportional to $1/\epsilon_b$ for $\epsilon_b < \epsilon_a$.

5 Closing remarks

When a random mixture of two isotropic dielectric materials, one composed of oriented spheroidal particles of relative permittivity ϵ_a and the other composed of oriented spheroidal particles of relative permittivity ϵ_b, is considered in the long wavelength regime, the resulting HCM is either an orthorhombic biaxial or a uniaxial dielectric material. The degree of anisotropy exhibited by the HCM depends upon the eccentricity of the constituent spheroidal particles, and it is greatest when the alignments of the two populations of spheroids are the same. The greatest degrees of HCM anisotropy are achieved when the constituent particles are shaped as needles or discs. In these instances, explicit formulas for the HCM anisotropy may be derived from the dyadic Bruggeman equation (4). Using these formulas at fixed values of volume fraction and ϵ_a, we find that the degrees of HCM anisotropy are proportional to $\sqrt{\epsilon_b}$ or ϵ_b for $\epsilon_b > \epsilon_a$, and proportional to $1/\sqrt{\epsilon_b}$ or $1/\epsilon_b$ for $\epsilon_b < \epsilon_a$. Thus, in principle, there is no limit to degree of anisotropy that may be attained via homogenization. In practice, the degree of anisotropy would be limited by the available value of ϵ_b (and/or ϵ_a). These findings may be helpful to those engaged in the development of anisotropic nanostructured composite materials for specific functions. For example, the described homogenization process may enable the very high degrees of anisotropy which are required to create material analogues for various curved spacetime [9, 10, 11, 12] and quantum electrodynamical [13] scenarios to be attained.

Owing to the electric–magnetic duality intrinsic to the Maxwell equations [19, 23], the findings presented herein apply equally well to magnetic properties. That is, by the homogenization of a random mixture of isotropic magnetic materials, distributed as oriented spheroidal particles, very high degrees of magnetic anisotropy may be attained.

Appendix

The double integrals on the right side of Eqs. (6) yield the depolarization dyadics $\underline{\underline{D}}_\ell$. Here we present evaluations of these integrals. Let us begin with case (i), wherein the HCM is an orthorhombic biaxial

dielectric material. By symmetry considerations, the off-diagonal terms of $\underline{\underline{D}}_\ell$ are null-valued; thus, we have the diagonal form

$$\underline{\underline{D}}_\ell = \left(\underline{\underline{U}}_\ell^{-1}\right) \bullet \left(\tilde{D}_\ell^x\, \hat{\underline{x}}\,\hat{\underline{x}} + \tilde{D}_\ell^y\, \hat{\underline{y}}\,\hat{\underline{y}} + \tilde{D}_\ell^z\, \hat{\underline{z}}\,\hat{\underline{z}}\right) \bullet \left(\underline{\underline{U}}_\ell^{-1}\right), \qquad (\ell = a, b)\,. \tag{17}$$

If we integrate the components $\tilde{D}_\ell^{x,y,z}$ first with respect to ϕ and then introduce the new variable $u = \cos\theta$, we find

$$\left.\begin{aligned} \tilde{D}_\ell^x &= \frac{1}{\tilde{\epsilon}_\ell^x - \tilde{\epsilon}_\ell^y}\left(1 - \int_0^1 du \sqrt{\frac{\tilde{\epsilon}_\ell^y + (\tilde{\epsilon}_\ell^z - \tilde{\epsilon}_\ell^y)\,u^2}{\tilde{\epsilon}_\ell^x + (\tilde{\epsilon}_\ell^z - \tilde{\epsilon}_\ell^x)\,u^2}}\right) \\ \tilde{D}_\ell^y &= \frac{1}{\tilde{\epsilon}_\ell^y - \tilde{\epsilon}_\ell^x}\left(1 - \int_0^1 du \sqrt{\frac{\tilde{\epsilon}_\ell^x + (\tilde{\epsilon}_\ell^z - \tilde{\epsilon}_\ell^x)\,u^2}{\tilde{\epsilon}_\ell^y + (\tilde{\epsilon}_\ell^z - \tilde{\epsilon}_\ell^y)\,u^2}}\right) \\ \tilde{D}_\ell^z &= \int_0^1 du \frac{u^2}{\sqrt{[\tilde{\epsilon}_\ell^x + (\tilde{\epsilon}_\ell^z - \tilde{\epsilon}_\ell^x)\,u^2]\,[\tilde{\epsilon}_\ell^y + (\tilde{\epsilon}_\ell^z - \tilde{\epsilon}_\ell^y)\,u^2]}} \end{aligned}\right\}, \quad (\ell = a, b)\,, \tag{18}$$

wherein

$$\tilde{\epsilon}_\ell^n = \frac{\epsilon_n}{(U_\ell^n)^2}, \qquad (\ell = a, b; n = x, y, z)\,, \tag{19}$$

with U_ℓ^n being the diagonal components of the shape dyadics $\underline{\underline{U}}_{a,b}$, i.e.,

$$\underline{\underline{U}}_\ell \equiv U_\ell^x\, \hat{\underline{x}}\,\hat{\underline{x}} + U_\ell^y\, \hat{\underline{y}}\,\hat{\underline{y}} + U_\ell^z\, \hat{\underline{z}}\,\hat{\underline{z}}, \qquad (\ell = a, b)\,. \tag{20}$$

The terms on the right sides in Eqs. (18) are expressible in terms of incomplete elliptic integrals; the form of these elliptic integral expressions depends upon the relative sizes of $\tilde{\epsilon}_\ell^x$, $\tilde{\epsilon}_\ell^y$ and $\tilde{\epsilon}_\ell^z$. For $\tilde{\epsilon}_\ell^{x,y,z} > 0$ we find

$$\tilde{D}_\ell^x = \begin{cases} \dfrac{1 + i\sqrt{\frac{\tilde{\epsilon}_\ell^y}{\tilde{\epsilon}_\ell^z - \tilde{\epsilon}_\ell^x}}\,E\left(i\sinh^{-1}\sqrt{\frac{\tilde{\epsilon}_\ell^z}{\tilde{\epsilon}_\ell^x} - 1}, \sqrt{\frac{\tilde{\epsilon}_\ell^x(\tilde{\epsilon}_\ell^y - \tilde{\epsilon}_\ell^z)}{\tilde{\epsilon}_\ell^y(\tilde{\epsilon}_\ell^x - \tilde{\epsilon}_\ell^z)}}\right)}{\tilde{\epsilon}_\ell^x - \tilde{\epsilon}_\ell^y}, & \begin{array}{l}\tilde{\epsilon}_\ell^z > \tilde{\epsilon}_\ell^y > \tilde{\epsilon}_\ell^x, \\ \tilde{\epsilon}_\ell^y > \tilde{\epsilon}_\ell^z > \tilde{\epsilon}_\ell^x, \\ \tilde{\epsilon}_\ell^z > \tilde{\epsilon}_\ell^x > \tilde{\epsilon}_\ell^y; \end{array} \\ \dfrac{1 - \sqrt{\frac{\tilde{\epsilon}_\ell^y}{\tilde{\epsilon}_\ell^x - \tilde{\epsilon}_\ell^z}}\,E\left(\sec^{-1}\sqrt{\frac{\tilde{\epsilon}_\ell^x}{\tilde{\epsilon}_\ell^z}}, \sqrt{\frac{\tilde{\epsilon}_\ell^x(\tilde{\epsilon}_\ell^y - \tilde{\epsilon}_\ell^z)}{\tilde{\epsilon}_\ell^y(\tilde{\epsilon}_\ell^x - \tilde{\epsilon}_\ell^z)}}\right)}{\tilde{\epsilon}_\ell^x - \tilde{\epsilon}_\ell^y}, & \begin{array}{l}\tilde{\epsilon}_\ell^y > \tilde{\epsilon}_\ell^x > \tilde{\epsilon}_\ell^z, \\ \tilde{\epsilon}_\ell^x > \tilde{\epsilon}_\ell^z > \tilde{\epsilon}_\ell^y, \\ \tilde{\epsilon}_\ell^x > \tilde{\epsilon}_\ell^y > \tilde{\epsilon}_\ell^z; \end{array} \end{cases} \tag{21}$$

$$\tilde{D}_\ell^y = \begin{cases} \dfrac{-1 - i\sqrt{\frac{\tilde{\epsilon}_\ell^x}{\tilde{\epsilon}_\ell^z - \tilde{\epsilon}_\ell^y}}\,E\left(i\sinh^{-1}\sqrt{\frac{\tilde{\epsilon}_\ell^z}{\tilde{\epsilon}_\ell^y} - 1}, \sqrt{\frac{\tilde{\epsilon}_\ell^y(\tilde{\epsilon}_\ell^x - \tilde{\epsilon}_\ell^z)}{\tilde{\epsilon}_\ell^x(\tilde{\epsilon}_\ell^y - \tilde{\epsilon}_\ell^z)}}\right)}{\tilde{\epsilon}_\ell^x - \tilde{\epsilon}_\ell^y}, & \begin{array}{l}\tilde{\epsilon}_\ell^z > \tilde{\epsilon}_\ell^y > \tilde{\epsilon}_\ell^x, \\ \tilde{\epsilon}_\ell^x > \tilde{\epsilon}_\ell^z > \tilde{\epsilon}_\ell^y, \\ \tilde{\epsilon}_\ell^z > \tilde{\epsilon}_\ell^x > \tilde{\epsilon}_\ell^y; \end{array} \\ \dfrac{-1 + \sqrt{\frac{\tilde{\epsilon}_\ell^x}{\tilde{\epsilon}_\ell^y - \tilde{\epsilon}_\ell^z}}\,E\left(\sec^{-1}\sqrt{\frac{\tilde{\epsilon}_\ell^y}{\tilde{\epsilon}_\ell^z}}, \sqrt{\frac{\tilde{\epsilon}_\ell^y(\tilde{\epsilon}_\ell^x - \tilde{\epsilon}_\ell^z)}{\tilde{\epsilon}_\ell^x(\tilde{\epsilon}_\ell^y - \tilde{\epsilon}_\ell^z)}}\right)}{\tilde{\epsilon}_\ell^x - \tilde{\epsilon}_\ell^y}, & \begin{array}{l}\tilde{\epsilon}_\ell^y > \tilde{\epsilon}_\ell^x > \tilde{\epsilon}_\ell^z, \\ \tilde{\epsilon}_\ell^y > \tilde{\epsilon}_\ell^z > \tilde{\epsilon}_\ell^x, \\ \tilde{\epsilon}_\ell^x > \tilde{\epsilon}_\ell^y > \tilde{\epsilon}_\ell^z; \end{array} \end{cases} \tag{22}$$

and

$$\tilde{D}_\ell^z = \begin{cases} \dfrac{F\left(\sec^{-1}\sqrt{\frac{\tilde{\epsilon}_\ell^x}{\tilde{\epsilon}_\ell^z}}, \sqrt{\frac{\tilde{\epsilon}_\ell^x\left(\tilde{\epsilon}_\ell^y-\tilde{\epsilon}_\ell^z\right)}{\tilde{\epsilon}_\ell^y\left(\tilde{\epsilon}_\ell^x-\tilde{\epsilon}_\ell^z\right)}}\right) - E\left(\sec^{-1}\sqrt{\frac{\tilde{\epsilon}_\ell^x}{\tilde{\epsilon}_\ell^z}}, \sqrt{\frac{\tilde{\epsilon}_\ell^x\left(\tilde{\epsilon}_\ell^y-\tilde{\epsilon}_\ell^z\right)}{\tilde{\epsilon}_\ell^y\left(\tilde{\epsilon}_\ell^x-\tilde{\epsilon}_\ell^z\right)}}\right)}{(\tilde{\epsilon}_\ell^y-\tilde{\epsilon}_\ell^z)\,\frac{\sqrt{\tilde{\epsilon}_\ell^x-\tilde{\epsilon}_\ell^z}}{\sqrt{\tilde{\epsilon}_\ell^y}}}, & \tilde{\epsilon}_\ell^y > \tilde{\epsilon}_\ell^x > \tilde{\epsilon}_\ell^z, \\ & \tilde{\epsilon}_\ell^x > \tilde{\epsilon}_\ell^z > \tilde{\epsilon}_\ell^y, \\ & \tilde{\epsilon}_\ell^x > \tilde{\epsilon}_\ell^y > \tilde{\epsilon}_\ell^z; \\ \dfrac{F\left(i\sinh^{-1}\sqrt{\frac{\tilde{\epsilon}_\ell^z-\tilde{\epsilon}_\ell^y}{\tilde{\epsilon}_\ell^y}}, \sqrt{\frac{\tilde{\epsilon}_\ell^y\left(\tilde{\epsilon}_\ell^z-\tilde{\epsilon}_\ell^x\right)}{\tilde{\epsilon}_\ell^x\left(\tilde{\epsilon}_\ell^z-\tilde{\epsilon}_\ell^y\right)}}\right) - E\left(i\sinh^{-1}\sqrt{\frac{\tilde{\epsilon}_\ell^z-\tilde{\epsilon}_\ell^y}{\tilde{\epsilon}_\ell^y}}, \sqrt{\frac{\tilde{\epsilon}_\ell^y\left(\tilde{\epsilon}_\ell^z-\tilde{\epsilon}_\ell^x\right)}{\tilde{\epsilon}_\ell^x\left(\tilde{\epsilon}_\ell^z-\tilde{\epsilon}_\ell^y\right)}}\right)}{(\tilde{\epsilon}_\ell^z-\tilde{\epsilon}_\ell^x)\,\frac{\sqrt{\tilde{\epsilon}_\ell^z-\tilde{\epsilon}_\ell^y}}{i\sqrt{\tilde{\epsilon}_\ell^x}}}, & \tilde{\epsilon}_\ell^z > \tilde{\epsilon}_\ell^y > \tilde{\epsilon}_\ell^x, \\ & \tilde{\epsilon}_\ell^z > \tilde{\epsilon}_\ell^x > \tilde{\epsilon}_\ell^y; \\ \dfrac{E\left(\sin^{-1}\sqrt{\frac{\tilde{\epsilon}_\ell^z-\tilde{\epsilon}_\ell^x}{\tilde{\epsilon}_\ell^z}}, \sqrt{\frac{\tilde{\epsilon}_\ell^x\left(\tilde{\epsilon}_\ell^y-\tilde{\epsilon}_\ell^z\right)}{\tilde{\epsilon}_\ell^y\left(\tilde{\epsilon}_\ell^z-\tilde{\epsilon}_\ell^x\right)}}\right) - F\left(\sin^{-1}\sqrt{\frac{\tilde{\epsilon}_\ell^z-\tilde{\epsilon}_\ell^x}{\tilde{\epsilon}_\ell^z}}, \sqrt{\frac{\tilde{\epsilon}_\ell^x\left(\tilde{\epsilon}_\ell^y-\tilde{\epsilon}_\ell^z\right)}{\tilde{\epsilon}_\ell^y\left(\tilde{\epsilon}_\ell^z-\tilde{\epsilon}_\ell^x\right)}}\right)}{(\tilde{\epsilon}_\ell^z-\tilde{\epsilon}_\ell^y)\,\frac{\sqrt{\tilde{\epsilon}_\ell^z-\tilde{\epsilon}_\ell^x}}{\sqrt{\tilde{\epsilon}_\ell^y}}}, & \tilde{\epsilon}_\ell^y > \tilde{\epsilon}_\ell^z > \tilde{\epsilon}_\ell^x. \end{cases} \tag{23}$$

The quantities $F(\varphi, k)$ and $E(\varphi, k)$ herein are the incomplete elliptic integrals of the first and second kind, respectively, as defined by [26]

$$\left.\begin{aligned} F(\varphi,k) &= \int_0^\varphi \frac{dt}{\sqrt{1-k^2\sin^2 t}} \\ E(\varphi,k) &= \int_0^\varphi \sqrt{1-k^2\sin^2 t}\,dt \end{aligned}\right\}, \tag{24}$$

with φ being the *amplitude*. For compact representation, imaginary-valued amplitudes are used in Eqs. (21)–(23), but all depolarization dyadic components herein are real-valued. Standard elliptic integral identities [27] may be used to re-express Eqs. (21)–(23) in terms of real-valued amplitudes. The expressions (21)–(23) represent a generalization of the corresponding results derived by Weiglhofer for spherical particles embedded in a biaxial dielectric material [22].

Now, we turn to case (ii) wherein the HCM is a uniaxial dielectric material. The depolarization dyadic retains the diagonal form (17) but here $\tilde{D}_\ell^x = \tilde{D}_\ell^y$. The integrals on the right sides of Eqs. (18) may be evaluated as

$$\tilde{D}_\ell^x = \frac{U_x^2}{\epsilon_x}\,\Gamma_x(\nu), \tag{25}$$

$$\tilde{D}_\ell^z = \frac{U_z^2\nu}{\epsilon_z}\,\Gamma_z(\nu), \tag{26}$$

wherein the terms

$$\Gamma_x(\nu) = \begin{cases} \frac{1}{2}\left(\frac{1}{1-\nu} - \frac{\nu \sinh^{-1}\sqrt{\frac{1-\nu}{\nu}}}{(1-\nu)^{\frac{3}{2}}}\right) & \text{for } 0<\nu<1 \\ \frac{1}{2}\left(\frac{\nu \sec^{-1}\sqrt{\nu}}{(\nu-1)^{\frac{3}{2}}} - \frac{1}{\nu-1}\right) & \text{for } \nu>1 \end{cases}, \tag{27}$$

$$\Gamma_z(\nu) = \begin{cases} \frac{\sinh^{-1}\sqrt{\frac{1-\nu}{\nu}}}{(1-\nu)^{\frac{3}{2}}} - \frac{1}{1-\nu} & \text{for } 0<\nu<1 \\ \frac{1}{\nu-1} - \frac{\sec^{-1}\sqrt{\nu}}{(\nu-1)^{\frac{3}{2}}} & \text{for } \nu>1 \end{cases}, \tag{28}$$

$$\tag{29}$$

with the scalar parameter

$$\nu = \frac{U_x^2 \epsilon_z}{U_z^2 \epsilon_x}. \tag{30}$$

The anomalous case $\nu < 0$, which corresponds to a hyperbolic HCM [28], is excluded from our consideration here.

References

[1] Givargizov E I 1987 *Highly Anisotropic Crystals* Springer, New York

[2] Wakaki M 2012 *Optical Materials and Applications* CRC Press, London

[3] Jiang W X, Chin J Y, Cui T J 2009 Anisotropic metamaterial devices *Materials Today* **12** 26–33

[4] Liu X, Li C, Yao K, Meng X and Li F 2009 Invisibility cloaks modeled by anisotropic metamaterials based on inductor-capacitor networks *Antennas Wireless Propagat. Lett., IEEE* **8** 1154 - 1157

[5] Mirala A and Abdolali 2013 A zero reflection from layered anisotropic metamaterial structures *Waves in Random and Complex Media* **23** 152–168

[6] Cheng Q, Jiang W X and Cui T J 2012 Spatial power combination for omnidirectional radiation via anisotropic metamaterials *Phys. Rev. Lett.* **108** 213903

[7] Podolskiy V A and Narimanov E E 2005 Strongly anisotropic waveguide as a nonmagnetic left-handed system *Phys. Rev. B* **71** 201101(R)

[8] Peng L, Ran L and Mortensen N A 2010 Achieving anisotropy in metamaterials made of dielectric cylindrical rods *Appl. Phys. Lett.* **96** 241108

[9] Smolyaninov I I 2003 Surface plasmon toy model of a rotating black hole *New J. Phys.* **5** 147

[10] Lu W, Jin J, Lin Z and Chen H 2010 A simple design of an artificial electromagnetic black hole *J. Appl. Phys.* **108** 064517

[11] Mackay T G and Lakhtakia A 2011 Towards a realization of Schwarzschild-(anti-)de Sitter spacetime as a particulate metamaterial *Phys. Rev. B* **83** 195424

[12] Mackay T G and Lakhtakia A 2010 Towards a metamaterial simulation of a spinning cosmic string *Phys. Lett. A* **374** 2305–2308

[13] Mackay T G and Lakhtakia A 2012 Towards an experimental realization of affinely transformed linearized quantum electrodynamics vacuum via inverse homogenization *J. Opt. Soc. America. B* **29** 1680–1684

[14] Mackay T G, Lakhtakia A and Weiglhofer W S 2001 Homogenisation of similarly oriented, metallic ellipsoidal inclusions using the bilocally-approximated strong-property-fluctuation theory *Opt. Commun.* **197** 89–95

[15] Ward L 2000 *The Optical Constants of Bulk Materials and Films, 2nd ed.* Institute of Physics, Bristol, UK

[16] Goncharenko A V 2003 Generalizations of the Bruggeman equation and a concept of shape-distributed particle composites *Phys. Rev. E* **68** 041108

[17] Mackay T G 2007 On the effective permittivity of silver–insulator nanocomposites *J. Nanophotonics* **1** 019501

[18] Duncan A J, Mackay T G and Lakhtakia A 2007 On the Bergman–Milton bounds for the homogenization of dielectric composite materials *Opt. Commun.* **271** 470–474

[19] Mackay T G and Lakhtakia A 2010 *Electromagnetic Anisotropy and Bianisotropy: A Field Guide* Word Scientific, Singapore

[20] Michel B 1997 A Fourier space approach to the pointwise singularity of an anisotropic dielectric medium *Int. J. Appl. Electromagn. Mech.* **8** 219–227

[21] Michel B and Weiglhofer W S 1997 Pointwise singularity of dyadic Green function in a general bianisotropic medium *Arch. Elekron. Übertrag.* **51** 219–223 Erratum 1998 **52** 31

[22] Weiglhofer W S 1998 Electromagnetic depolarization dyadics and elliptic integrals *J. Phys. A: Math. Gen.* **31** 7191–7196

[23] Mackay T G and Lakhtakia 2008 Electromagnetic fields in linear bianisotropic mediums *Progress in Optics* **51** 121–209

[24] Weiglhofer W S and Mackay T G 2002 Needles and pillboxes in anisotropic mediums *IEEE Trans. Antennas Propagat.* **50** 85–86

[25] Cottis P G, Vazouras C N and Spyrou C 1999 Green's function for an unbounded biaxial medium in cylindrical coordinates *IEEE Trans. Antennas Propagat.* **47** 195–199

[26] Gradshteyn I S and Ryzhik I M (Eds. Jeffrey A and Zwillinger D) 2007 *Table of Integrals, Series, and Products, 7th edition* Academic Press, Burlington, MA

[27] Abramowitz M and Stegun I A 1972 *Handbook of Mathematical Functions with Formulas, Graphs, and Mathematical Tables* Dover, New York

[28] Mackay T G, Lakhtakia A and Depine R A 2006 Uniaxial dielectric media with hyperbolic dispersion relations *Microwave Opt. Technol. Lett.* **48** 363–367

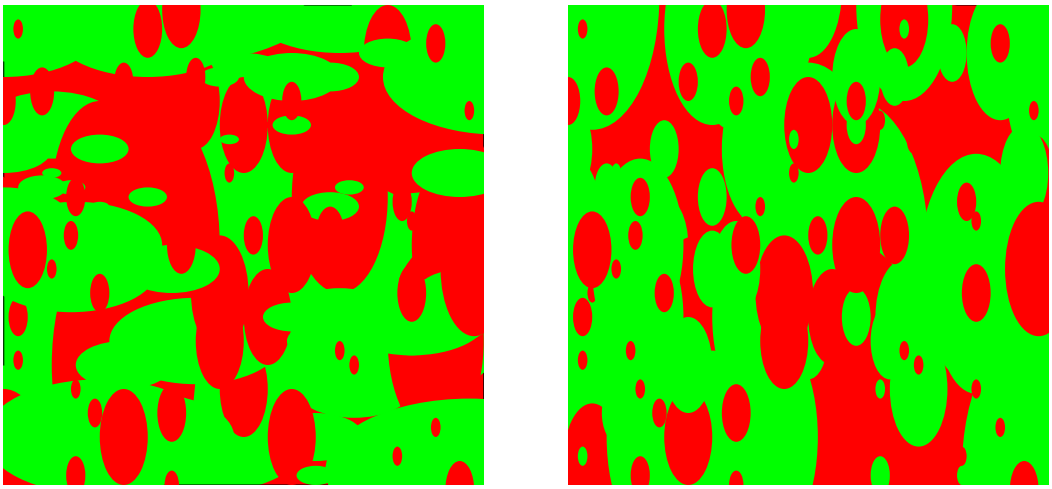

Figure 1: Two schematic representations of randomly-mixed component material a and b spheroids. The component material a spheroids all have the same orientation and the component material b spheroids all have the same orientation; we consider cases wherein these two orientations are mutually perpendicular (left) and are the same (right).

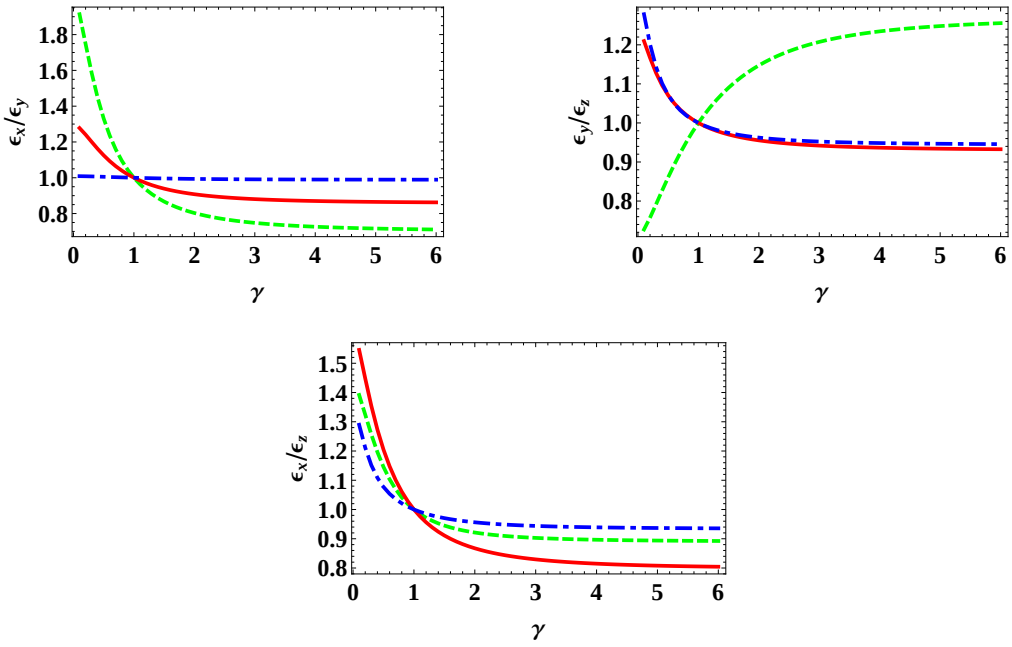

Figure 2: ϵ_x/ϵ_y, ϵ_y/ϵ_z and ϵ_x/ϵ_z plotted versus the eccentricity parameter $\gamma \in (0.1, 6)$ for volume fractions $f_a = 0.7$ (green, dashed curves), 0.4 (red, solid curves) and 0.1 (blue, broken dashed curves). The symmetry axis of the component a spheroids is parallel to the z coordinate axis whereas the symmetry axis of the component b spheroids is parallel to the y coordinate axis.

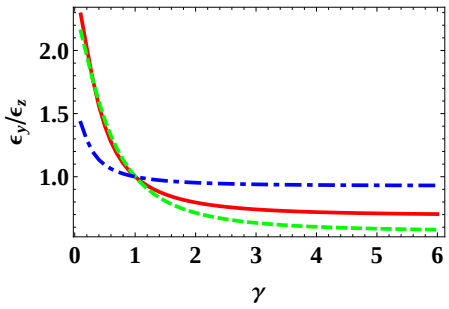

Figure 3: ϵ_y/ϵ_z plotted versus the eccentricity parameter $\gamma \in (0.1, 6)$ for volume fractions $f_a = 0.7$ (green, dashed curve), 0.4 (red, solid curve) and 0.1 (blue, broken dashed curve). The symmetry axes of the component a and b spheroids are parallel to the z coordinate axis.

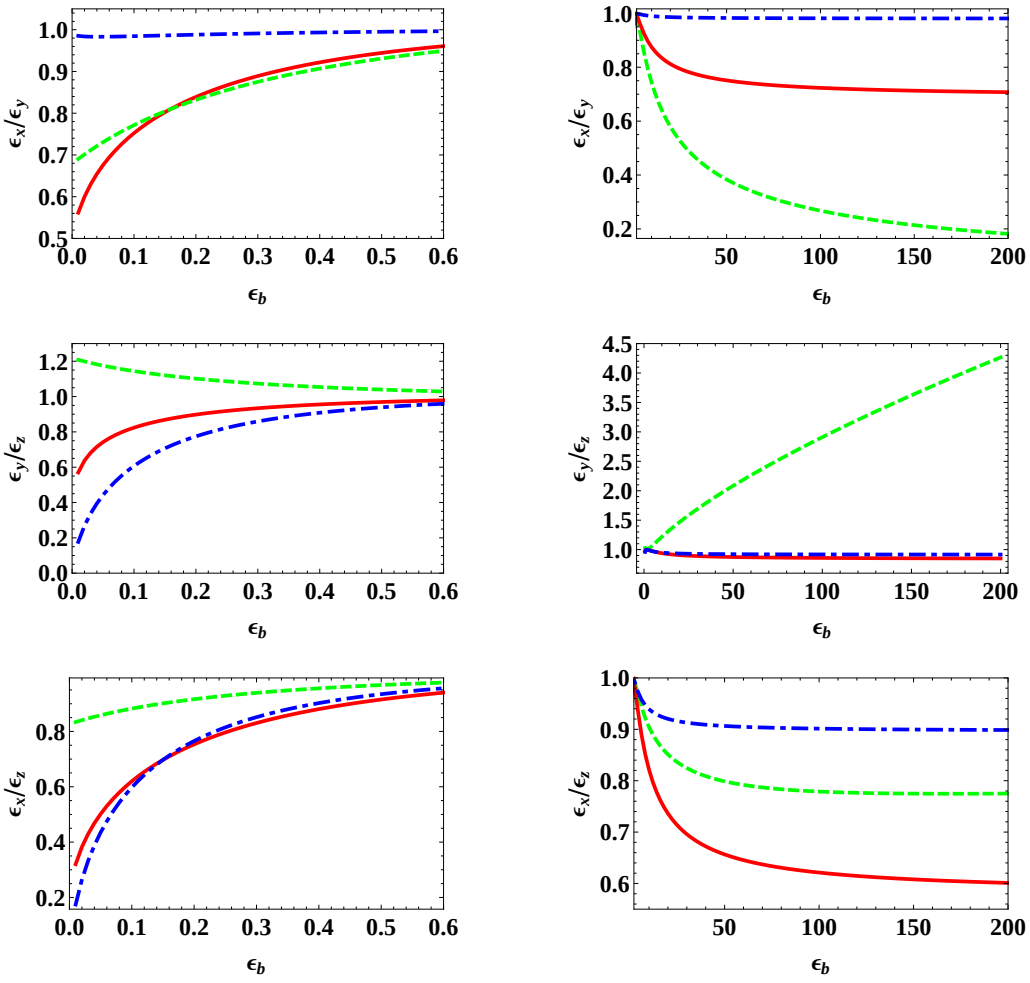

Figure 4: ϵ_x/ϵ_y, ϵ_y/ϵ_z and ϵ_x/ϵ_z plotted versus $\epsilon_b \in (0.01, 0.6)$ (left) and $(0.6, 200)$ (right) for volume fractions $f_a = 0.7$ (green, dashed curves), 0.4 (red, solid curves) and 0.1 (blue, broken dashed curves). The component a needles are parallel to the z coordinate axis whereas the component b needles are parallel to the y coordinate axis.

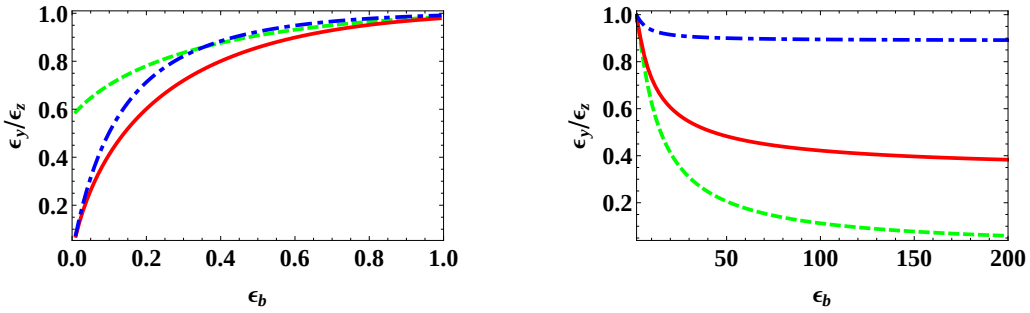

Figure 5: ϵ_y/ϵ_z plotted versus $\epsilon_b \in (0.01, 1)$ (left) and $(1, 200)$ (right) for volume fractions $f_a = 0.7$ (green, dashed curves), 0.4 (red, solid curves) and 0.1 (blue, broken dashed curves). The component a and b needles are both parallel to the z coordinate axis.

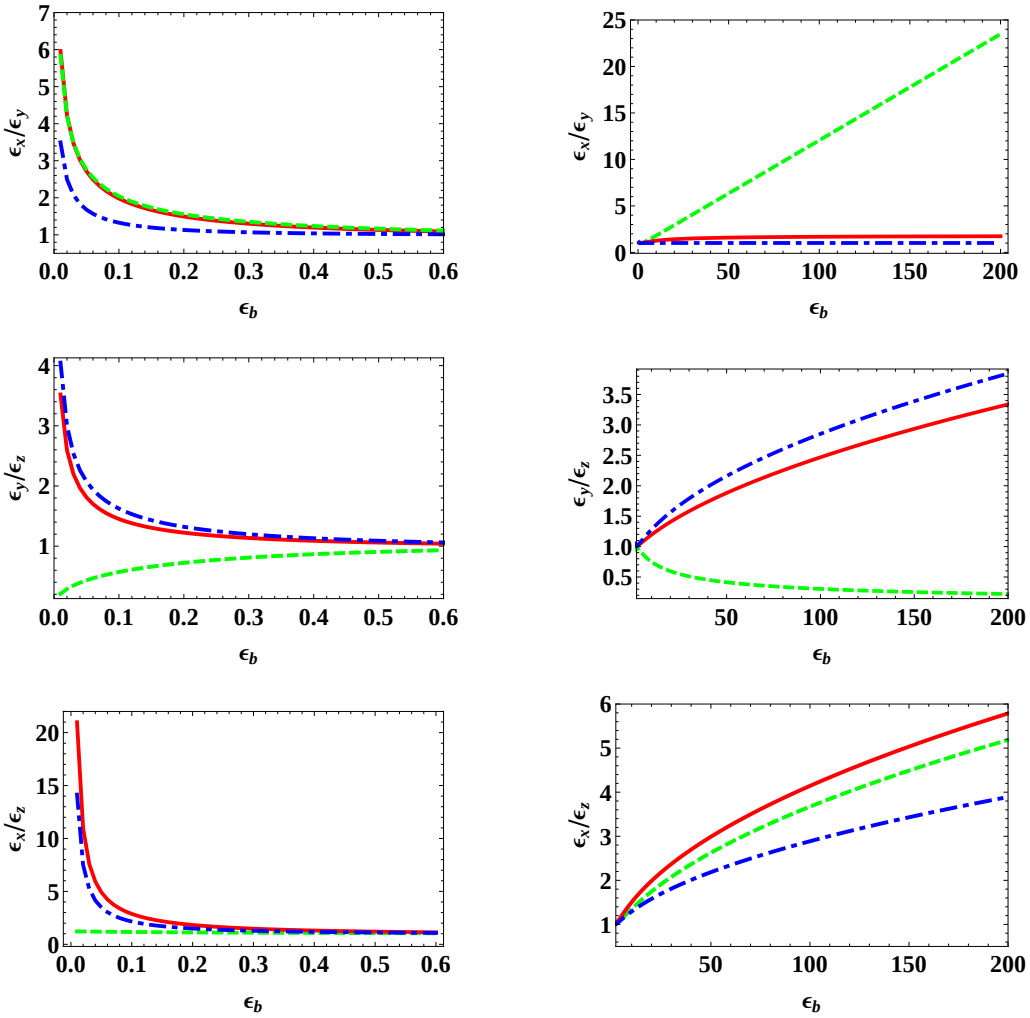

Figure 6: ϵ_x/ϵ_y, ϵ_y/ϵ_z and ϵ_x/ϵ_z plotted versus $\epsilon_b \in (0.01, 0.6)$ (left) and $(0.6, 200)$ (right) for volume fractions $f_a = 0.7$ (green, dashed curves), 0.4 (red, solid curves) and 0.1 (blue, broken dashed curves). The component a discs are parallel to the xy coordinate plane whereas the component b discs are parallel to the xz coordinate plane.

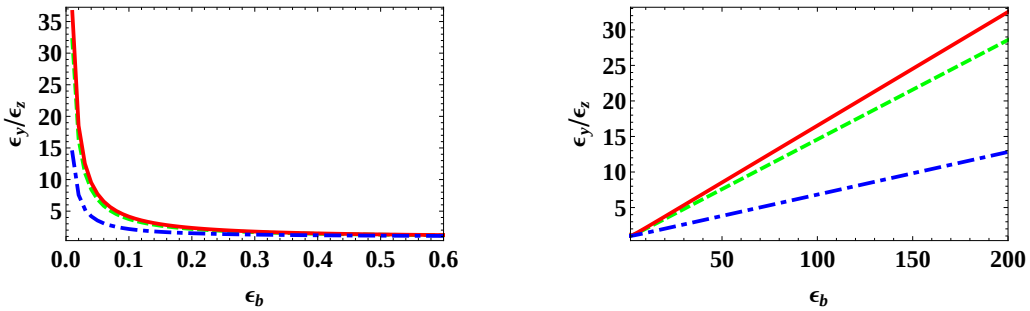

Figure 7: ϵ_y/ϵ_z plotted versus $\epsilon_b \in (0.01, 0.6)$ (left) and $(0.6, 200)$ (right) for volume fractions $f_a = 0.7$ (green, dashed curves), 0.4 (red, solid curves) and 0.1 (blue, broken dashed curves). The component a and b discs are both parallel to the xy coordinate plane.